Quantification of Pulse-Dependent Trabecular Meshwork Motion in Normal Humans Using Phase-Sensitive OCT

Chen Xin,[1] Shaozhen Song,[2] Murray Johnstone,[3] Ningli Wang,[1] and Ruikang K. Wang[2,3]

[1]Beijing Institute of Ophthalmology, Beijing Tongren Eye Center, Beijing Tongren Hospital, Capital Medical University, Beijing, China
[2]Department of Bioengineering, University of Washington, Seattle, Washington, United States
[3]Department of Ophthalmology, University of Washington, Seattle, Washington, United States

Correspondence: Ruikang K. Wang, Department of Bioengineering, University of Washington, Seattle, WA 98195, USA; wangrk@uw.edu.

Submitted: December 8, 2017
Accepted: May 30, 2018

Citation: Xin C, Song S, Johnstone M, Wang N, Wang RK. Quantification of pulse-dependent trabecular meshwork motion in normal humans using phase-sensitive OCT. *Invest Ophthalmol Vis Sci*. 2018;59:3675–3681. https://doi.org/10.1167/iovs.17-23579

Purpose. The purpose of this study was to characterize the pulsatile motion of trabecular meshwork (TM) in normal subjects and demonstrate its changes in accommodation with phase-sensitive optical coherence tomography (PhS-OCT).

Methods. A new PhS-OCT laboratory prototype was designed to measure pulsatile TM motion in 13 healthy humans. Two sets of images were captured in 10 subjects, first with best corrective refraction and the other with an additional 3.0 diopters of accommodation. In each image, both maximum velocity (MV) and cumulative displacement (CD) in two selected regions of TM, the internal (IMV and ICD) and external (EMV and ECD) region, were measured.

Results. For all parameters the intraclass correlation coefficient was >0.75. Neither MV nor CD was significantly different between eyes in individual subjects ($P_{IMV} = 0.967$, $P_{EMV} = 0.391$, $P_{ICD} = 0.603$, $P_{ECD} = 0.482$). In 26 eyes, with best corrective refraction, the EMV was higher than the IMV (23.9 ± 9.8 vs. 18.9 ± 8.08 μm/s; $P = 0.0001$), as was the ECD compared with the ICD (0.340 ±0.125 vs. 0.264 ± 0.111 μm; $P = 0.000004$). With accommodation, MV and CD significantly increased ($P_{IMV} = 0.0003$, $P_{EMV} = 0.0003$, $P_{ICD} = 0.019$, and $P_{ECD} = 0.007$), whereas MV and CD in the external region were still larger than those in the internal area ($P_{EMV\ vs.\ IMV} = 0.009$, $P_{ECD\ vs.\ ICD} = 0.023$).

Conclusions. This study demonstrates the differences in TM motion between the internal and external regions of TM and displays its change with accommodation. The findings and good reproducibility suggest PhS-OCT helps to understand TM function in regulation of IOP, and, with further refinements, it may be useful in clinical management of glaucoma.

Keywords: phase-sensitive OCT, trabecular meshwork, accommodation, pulsatile aqueous flow

Primary open angle glaucoma (POAG) is an insidious and irreversible leading cause of blindness. By 2040, 111.8 million people worldwide will have glaucoma. High IOP is the only recognized predisposing cause for POAG that is amendable to intervention. Trabecular meshwork (TM) pathways regulate aqueous humor drainage and maintain IOP within a normal range. Recent studies indicate that the TM pathway works as a unified organ system[1–3] through identification of pulsatile flow (PF) pattern in the aqueous veins (AV).[4,5] PF of aqueous is synchronous with the ocular pulse, which is generated by cardiac-induced pulsatile ocular blood flow into the choroid.[6,7] TM motion in response to the ocular pulse is determined by TM stiffness.[3] PF abnormalities are well documented in glaucoma and regarded as an indicator of increased TM stiffness.[3]

It is widely shown that significant changes in the components of the extracellular matrix (ECM) and in TM cellularity contributes to the change in TM tissue-level biomechanical properties.[8–10] Studies of isolated tissue have found TM stiffness to be considerably higher in POAG eyes.[10–12] The studies conclude that quantification of TM stiffness may represent a means of differentiating normal and POAG eyes.[13,14] However, ex vivo studies are unable to provide estimates of in vivo TM stiffness or TM interaction with surrounding tissues that may be important clinically.

One of the primary goals of imaging in the glaucoma arena is the development of tools that could eventually be adopted to improve care of glaucoma patients. Development of such tools requires, first, to demonstrate that the technology can image the appropriate target; second, to determine whether the results can be quantified; third, to characterize the behavior in normal subjects; and finally, to perform comparison of the findings in normal subjects with those in glaucoma.

Phase-sensitive optical coherence tomography (PhS-OCT)[15,16] has been documented to permit identification of a synchrony between time-dependent peaks of the ocular pulse and TM motion.[17,18] However, quantification of TM motion in vivo, variability among normal subjects, and reproducibility of the technique have not been previously reported. The additional steps necessary to determine the value of the PhS-OCT technology and its potential role in management of glaucoma require that baseline data in normal subjects first be obtained.

To bridge this knowledge gap, we describe a noninvasive imaging technique, PhS-OCT, to quantify the TM motion in vivo;

TM motion is a reflection of the biomechanical properties of TM tissues that would change depending on tissue stiffness. In the current PhS-OCT study, we characterize (1) the TM motion in a series of healthy young subjects, (2) comparison of internal and external regions of the TM motion, and (3) the effect of accommodation on TM motion.

Methods

Subjects

We recruited 13 healthy young individuals without any ocular diseases, trauma, or history of surgery. All participants underwent an examination including blood pressure, pulse, visual acuity, Goldmann applanation tonometry, refraction, slit-lamp biomicroscopy, and dilated fundus examination. The study was conducted under a protocol approved by the institutional review board of the University of Washington (UW; Seattle, WA, USA). Written informed consent was obtained from all participants, and the study adhered to the tenets of the Declaration of Helsinki and was conducted in compliance with the Health Insurance Portability and Accountability Act.

Imaging Acquisition and Scanning Protocol

The PhS-OCT laboratory prototype is composed of three parts (Fig. 1): (1) spectral domain OCT (SD-OCT) to capture the TM structure and motion, (2) a digital pulsimeter (ML 866; PowerLab, Colorado Springs, CO, USA) for recording the pulsed cardiac signal, and (3) an external controlling unit with two triggers to synchronize OCT data acquisition and cardiac signal recording. The digital pulsimeter was equipped with a piezo-electric transducer to convert the arterial pulse from the finger into an electrical analog signal.

The PhS-OCT system was based on the SD-OCT configuration, but the acquisition setup was equipped with an algorithm to extract the sensitive phase signal from the acquired time-resolved OCT datasets. The details of the PhS-OCT setup and the phase information extraction algorithm were described elsewhere.[18] To resolve the small tissue motion within the outflow tract while minimizing the bulk tissue motion artifacts, it is essential to reduce the imaging time interval between adjacent B-scans for the evaluation of tissue displacement in vivo. We found that the optimal time interval was approximately 2.5 ms (i.e., 400 frames/s) in our human subject study. In the meantime, to further suppress the motion artifacts, we improved the postprocessing algorithm to precisely and automatically align the adjacent B-scans to minimize undesired errors induced by pixel mismatch between B-frames. These new improvements were implemented in the system setup used in this study. During imaging, the incident light power in the sample arm used was 1.8 mW, within the safe ocular exposure limits recommended by the American National Standards Institute (ANSI).

While imaging, the head of the subject was placed on the slit-lamp style chin and headrest support. The slit-lamp style system contained a targeting light and a refractive error adjustment apparatus (REAA) (Haig Streit, Mason, OH, USA) that can induce accommodation. The temporal TM region was scanned in the examined eye. When imaging, the examined eye was rotated nasally by having the fellow eye fixed on the targeting light. The fixed orientation was established when scleral surface in the real-time B-scan image was tangent to the reference line displayed on the computer screen. Lenses were placed between the subject and the light source to provide the best corrected refraction and PhS-OCT measurements were acquired. Accommodation was then induced by adjusting the REAA to 3 diopters (D) in front of the targeting light, and PhS-OCT measurements were then again obtained under accommodative conditions.

Each dataset contained 2000 OCT B-scans (400 B-scans/s, 5-second duration) captured at a single cross-sectional position in the limbus area. The 2000 B-scans assemble an M-mode scan. A digital pulsimeter was placed on the tip of the index finger of the subjects, and concurrent pulse reading was assured by means of a trigger activating the OCT and pulsimeter simultaneously. Three repeated datasets were captured in individual eyes, and an identical scanning protocol was repeated on a separate day.

Both eyes in 10 of 13 participants (20 eyes) were imaged in two different states of refraction at a visit: one with best corrective refraction and the other with three-dimensional accommodation.

Data Processing

On a structural image, the hyporeflective schlemm's canal (SC) was identified at external side of the triangular TM. The investigator (CX) doing the analysis was masked to the accommodative status of the participants. Two regions of TM were selected (Fig. 2). The internal TM area was selected as a position one third of the distance anterior to the sclera spur (SS) along the inner margin of the TM adjacent to the anterior chamber (AC). The external TM region was selected as the point next to SC.

All the acquired M-mode scans were processed with a PhS-OCT algorithm[18] to extract the maximum velocity (MV) and the cumulative displacement (CD) of the TM tissue during a cardiac cycle. In brief, the data are processed as follows (Fig. 3): the OCT image was first constructed as a stack of B-scans, forming a M-mode data set of 2000 images (5-second duration). One representative OCT intensity image is displayed in Figure 3A. The phase shift in OCT signals was then calculated between adjacent B-scans followed by a phase compensation procedure to remove bulk tissue motion caused by involuntary movements of the eye and head during imaging. On each pixel, the instantaneous velocity (i.e., displacement between two B-scan images) was derived from the compensated OCT phase signals. After this procedure, the velocity waveform during the 5-second acquisition time window was obtained on every location. TM motion waveforms were then correlated with cardiac cycle, where the heart beat frequency and their harmonic frequencies were used to create a mask to filter the TM motion waveforms in frequency domain (Fig. 3B). MV was the maximum value on the velocity waveform. CD was the total motion amplitude within one cardiac cycle, calculated from the integration of velocity waveform. Finally, MV and CD were assessed at the individual selected locations. Both MV and CD at the internal (IMV and ICD) and external (EMV and ECD) locations were then analyzed.

A color representation of the changes in instantaneous velocity (i.e., the displacement between two B-scans) was overlaid onto the structural image to demonstrate the location of tissue motion in real time. In the color representation of velocity map, the warmer color (in red) indicates that the tissue is moving outward away from the OCT probe into SC and toward the sclera, whereas the cooler color (in blue) indicates the TM is moving inward away from the OCT probe toward the AC (Fig. 3C).

Statistics

All statistical analysis was done using SPSS 23.0 (IBM, New York, NY, USA). The intra-class correlation coefficient (ICC)

Investigative Ophthalmology & Visual Science

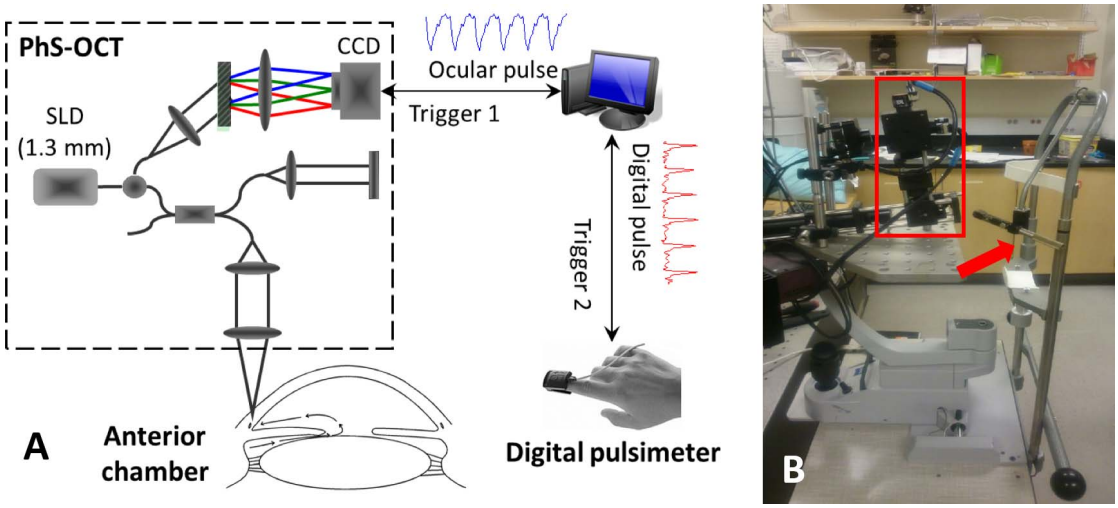

FIGURE 1. (**A**) The schematic system setup for the TM motion detection and (**B**) photograph of the laboratory prototype used in study. The system is composed of three parts noted in **A**: 1, SD-OCT for detecting TM tissue motion; 2, a digital pulsimeter connected to the index figure of the imaged subject; and 3, the computer working as an external controlling unit to send the triggers to synchronize OCT and pulse data. In **B**, the *red arrow* indicates the target for fixation when the subjects were examined. The target light is capable of refraction adjustment. The *red square* frames the SD-OCT scanning system.

was used to evaluate the reliability and repeatability of each measured parameter. In each subject, three continuous datasets captured on the same day followed by two additional datasets captured on separate days were used to test the repeatability and reliability of the PhS-OCT technique. An independent *t*-test was used to compare the tissue movement between the two eyes of individual subjects. A paired *t*-test was done to compare baseline MV and CD at the external and internal TM regions and to compare individual locations before and after accommodation. A multilogistic regression was used to analyze the relationship among blood pressure (BP), heart rate, IOP, and the parameters representing TM motion. $P < 0.05$ was considered statistically significant.

RESULTS

Thirteen healthy subjects (26 eyes) of seven males and six females with a mean age of 27.85 years (SD, ±3.34) were recruited in this study. The mean systolic BP (SBP) and diastolic BP (DBP) were 108 ± 10 and 73 ± 6 mm Hg (SD), respectively. The heart rate was 69 ± 11 beats per minute (SD). The mean IOP was 15.0 mm Hg ± 2.5 and 15.6 ± 0.6 mm Hg (SD) in the right and left eyes, respectively ($P = 0.150$). The mean refractive correction was −1.90 ± 0.81 D for the right eye and −1.65 ± 0.89 D (SD) for the left eye. No significant difference was found between eyes ($P = 0.171$).

Repeatability and Reliability Evaluation

The ICCs of IMV, EMV, ICD, and ECD for the three continuous scans in the same region were 0.953, 0.937, 0.917, and 0.914, respectively. The ICCs of IMV, EMV, ICD, and ECD for the two images captured on separated days were 0.973, 0.884, 0.913, and 0.782, respectively. Furthermore, the ICCs of IMV, EMV, ICD, and ECD for the three measurements of the same image were 0.976, 0.981, 0.962, and 0.984, respectively.

Twenty eyes from 10 healthy subjects were included for the comparative measurement of the TM motion with and without of accommodation. The mean age was 26.5 ± 2.43 years. The mean IOP was 15.0 mm Hg ± 2.5 mm Hg (SD) in the right eye and 15.6 ± 0.6 mm Hg (SD) in the left eye, with no significant difference between eyes ($P = 0.510$). The mean refraction correction between eyes was not significantly different ($P = 0.404$): −1.86 ± 0.86 D in the right eye and −1.65 ± 0.91 D (SD) in the left eye.

For the 13 healthy patients with best corrective refraction, the IMV and EMV in the right eye were 17.8 ± 7.1 and 23.0 ± 10.3 μm/s (SD), respectively, which was similar to the left eye: IMV was 20.0 ± 9.0 μm/s and EMV was 24.8 ± 10.7 μm/s (SD) ($P_{IMV} = 0.967$ and $P_{EMV} = 0.391$). The ICD and ECD in the right eye was 0.245 ± 0.103 and 0.328 ± 0.126 μm (SD), which was similar as that in the left eye: ICD was 0.294 ± 0.121 μm and ECD was 0.283 ± 0.119 μm (SD) ($P_{ICD} = 0.603$ and $P_{ECD} = 0.482$). In each eye, the MV and CD in the external TM region (EMV: 23.9 ± 9.8 μm/s; ECD: 0.340 ± 0.125 μm) are significantly higher than those in the internal region (IMV: 18.9 ± 8.08 μm/s and ICD: 0.264 ± 0.111; $P_{MV} = 0.0001$ and $P_{CD} = 0.000004$). The MV and CD showed no significant

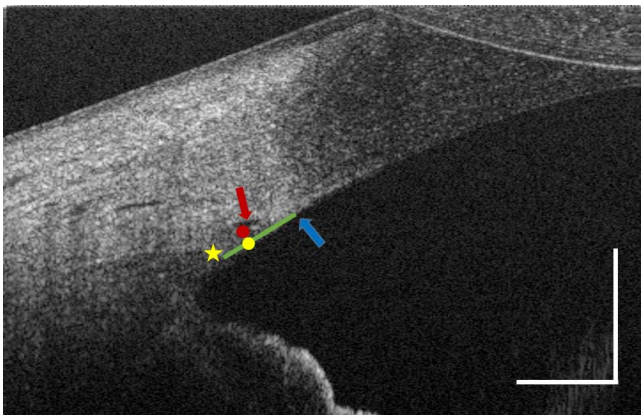

FIGURE 2. The selections of the region of interest for analysis. The *red circle* indicates the external TM region, next to Schlemm's canal. The *yellow star* points to the scleral spur, the *blue arrow* points to the Schwalbe's line and the *green line* indicates the internal length of the TM. The *yellow circle* indicates the internal TM region, which is one third of the distance anterior to scleral spur along the inner margin of the TM adjacent to the anterior chamber.

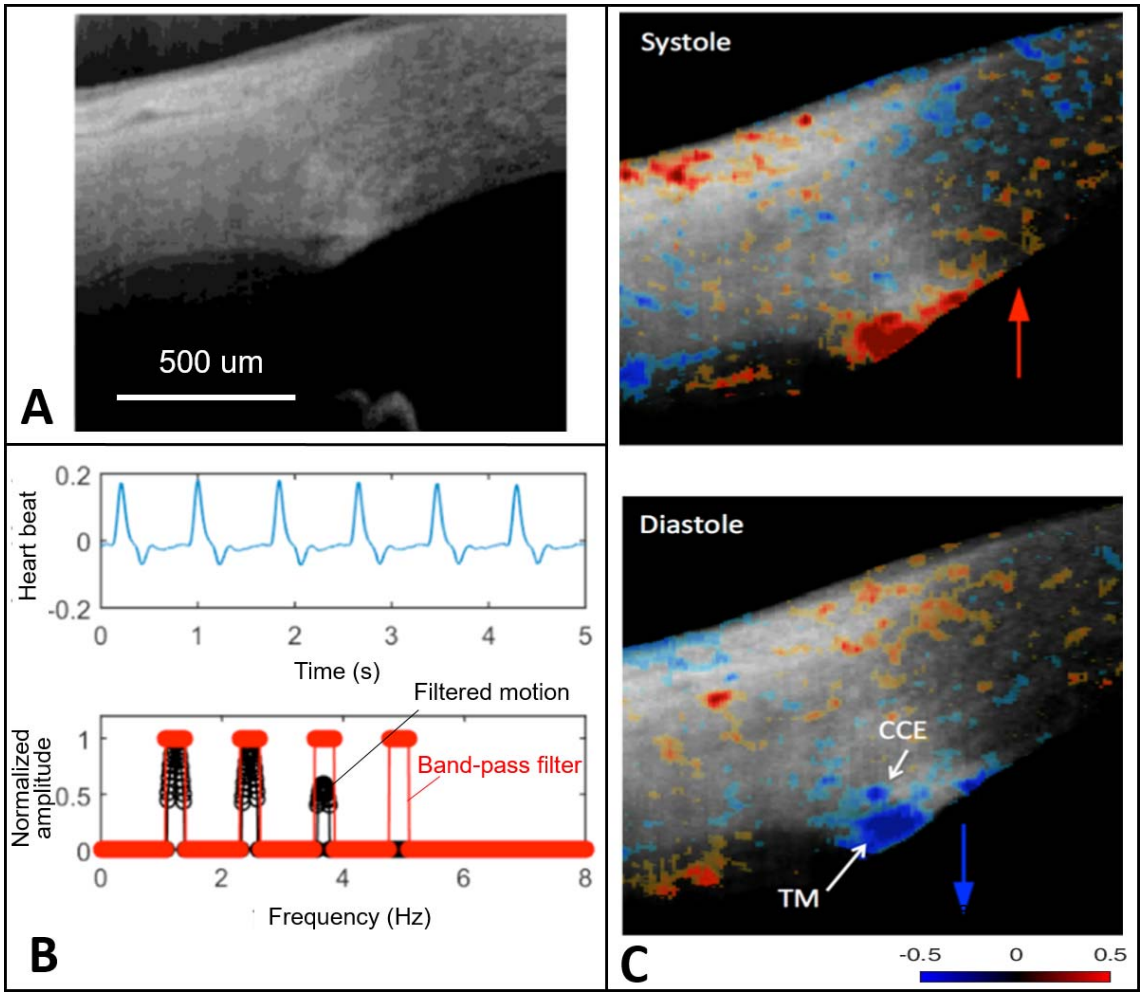

FIGURE 3. Data processing procedures. (**A**) Representative structural image captured by the OCT system. (**B**) Heart beat signals from a digital pulsimeter and its frequency domain positions (*red markings*). *Black trace* is the filtered TM motion signal, according to the heart beat signals. (**C**) Color-encoded instantaneous velocity overlaid on the structural image. The *red color* indicates the tissue movement anteriorly to the scleral surface, whereas the *blue color* indicates the tissue movement posteriorly to the anterior chamber.

relationship with blood pressure ($P_{SBP} = 0.876$ and $P_{DBP} = 0.539$), refraction ($P = 0.332$), and IOP ($P = 0.435$).

For 20 eyes further receiving the 3 D of accommodation, the parameter measurements with best corrective refraction were as follows: IMV = 18.8 ± 8.3 μm/s, EMV = 22.6 ± 7.7 μm/s, ICD = 0.281 ± 0.111 μm, and ECD = 0.353 ± 0.118 μm (SD). The MV and CD in the external region remained much higher than that in the internal area ($P_{MV} = 0.001$ and $P_{CD} = 0.000088$). With accommodating load, sharing the similar rate of change ($P = 0.692$), the EMV and IMV increased by 25.4% (28.5 ± 11.8 μm/s) and 23.1% (23.0 ± 10.0 μm/s), which is significantly higher than that with best corrective refraction ($P_{IMV} = 0.0003$, $P_{EMV} = 0.0003$). The EMV is still higher than IMV ($P = 0.009$). The ECD increased by 13.3% (0.401 ± 0.158 μm) and ICD by 16.7% (0.322 ± 0.138), which are significantly higher than that with best corrective refraction ($P_{ICD} = 0.019$ and $P_{ECD} = 0.007$). The increase rate was similar for ECD and ICD ($P = 0.588$), but ECD continued to be markedly higher than ICD after accommodation ($P = 0.023$).

DISCUSSION

Our study is unique in that it is the first time that parameters of pulse-dependent TM motion in a series of human eyes were characterized; a comparison of pulse-dependent motion in the inner and outer portions of the TM was done; and a comparison of pulse-dependent TM motion before and after accommodation was done. We found good reproducibility and reliability using ICC, allowing us to characterize MV and CD values in the series of normal eyes. The velocity of motion in the external TM was greater than that in the internal TM; for example, in the right eye, EMV > IMV by 29.2%, and in the left eye, EMV > IMV by 24% with the CD following a similar pattern. Following accommodation, TM motion increased, and its differences between diverse regions were still present and reached significance.

Aqueous outflow that determines IOP is the only parameter known by clinicians to slow the progression of glaucoma, yet practical clinical tools to assess the functional status of the aqueous outflow system are not available. We need better tools that can provide guidance relative to the outflow system status to diagnose and initiate rational treatment. We also need tools to provide feedback to tell us whether our medical management and surgery are effective.

The TM is situated in the scleral sulcus, extending from Schwalbe's line to the SS. TM cells contain actin networks, noncanonical Wnt signaling, and the Rho family of proteins, which have been closely linked to the function of stress fibers

and the contractile machinery of the cell.[19–21] TM cell and ECM stiffness determines TM motion, an important regulator of IOP homeostasis. Alterations in TM elasticity and compliance are likely the factors causing IOP elevation that leads to optic nerve damage in glaucoma. Clinical and laboratory studies provided evidence that the TM can sense and react to the biomechanical environment resulting from IOP fluctuations or cyclic IOP changes.[22–25] TM motion is an indicator of the TM biomechanical properties in vivo, which we demonstrate for the first time, can be reproducibly measured and characterized with our PhS-OCT technique.

Our study provides evidence of good reliability and repeatability of the PhS-OCT technique for quantifying TM motion in living healthy subjects. The TM motion is a direct reflection of the TM stiffness in vivo. Recently, several new glaucoma therapies targeting reconstruction of TM biomechanics are being developed for clinical application.[26,27] Our PhS-OCT technique may potentially be a promising tool to detect the presence of a TM abnormalities and optimize the selection of the operative site for minimally invasive glaucoma surgery (MIGS).

Relative motion of TM constituents in response to the ocular pulse has not previously been explored. The TM is divided into three parts: uveal meshwork, corneoscleral meshwork, and juxtacanulicular connective tissue (JCT). The mechanical properties of corneoscleral and uveal meshwork are determined by highly organized collagen and elastin constituents.[28–30] The corneoscleral meshwork consists of large parallel beams anchored to Schwalbe's line anteriorly and to the SS and ciliary body (CB) posteriorly; in contrast, the outer trabeculae near SC are much smaller, not organized in parallel sheets or beams and they are anchored to inner beams rather than to the anterior and posterior attachments. In addition, the JCT region contains much more loosely arranged extracellular matrix materials and elastic-like fibers.[31–35] Given the differences in constituent properties of the TM regions that govern biomechanical responses, one might expect differences in response to pressure changes induced by cyclic pulsatile flow.

In ex vivo eyes, when the perfusion pressure in the anterior chamber increases, the external region of the TM distends into the lumen of SC; when the pressure decreases, the TM previously distending into SC recoils to its original configuration.[36,37] Although the external region of TM is undergoing large excursions, the internal area of TM remains relatively stable.

The TM motion in the external TM region is much more prominent than that in the internal region. TM regions each have a unique geometry and composition that may be expected to confer different mechanical properties with associated differences in responses to pressure from the cyclic ocular pulse amplitude. The greater TM motion in the external region of the TM nearer SC suggests it may play a more active role than the internal TM in regulating and controlling aqueous outflow and IOP.

Our study also demonstrates an effect of accommodation on TM motion in vivo for the first time. With accommodation, the CB contracts anteriorly and circumferentially, which relaxes tension on the zonules attached to the lens, leading to the relaxation of the lens capsule.[38–40] The TM attaches to the CB and SS, so when accommodation is induced, the TM is pulled internally and anteriorly. The resultant vector forces increase spaces between the trabecular lamellae and enlarge the dimensions of SC lumen, collector channel entrances (CCE), and intrascleral channels. Tension on the CB and SS that pulls the TM away from SC wall also permits greater excursions of the TM.[41–43] Therefore, with accommodation load, the MV and CD in both the internal and external locations of the TM increased significantly. However, the pattern of the TM motion (i.e., the external TM moves stronger than the internal region) remains.

Many reports indicated that TM stiffness plays an important role in the pathologic changes in glaucoma. Changes in cellularity and extracellular matrix elements are associated with the glaucoma process in both animal models and in glaucoma patients.[44–50] Pulsatile aqueous flow progressively decreases and is eventually lost as the glaucoma process worsens.[44–46] In glaucoma patients, miotics transiently restore pulsatile aqueous flow into episcleral veins followed by a drop in IOP that persists throughout the duration of action of the drug. However, in advanced glaucoma, miotics fail to improve aqueous outflow and IOP.[47–50]

Restoration of pulsatile flow is consistent with transient recovery of TM motion. Pulsatile aqueous flow originates in SC and is synchronous with the cardiac and ocular pulse.[6,7] Pulsatile aqueous discharge from SC requires changes in SC lumen dimensions that can be explained by pulse pressure transferred across the TM. Active TM movement is thus required to transfer the ocular pulse pressure to SC. Alterations in TM stiffness will interfere with the ability to transfer the ocular pulse pressure to the canal.

The TM motion captured by our PhS-OCT technique is reflective of the functional behavior of the aqueous outflow pathways; deterioration of normal motion is related to the onset and severity of glaucoma. The ability to identify and quantitate TM movement should provide a means to assist in diagnosing, monitoring progression and choosing treatment options in glaucoma.

In the last decade, MIGSs have become an increasingly attractive choice. The MIGS choice is driven by reasonable efficacy balanced by low morbidity compared with traditional filtering procedures and drainage devices. Of special interest are MIGSs that bypass the TM providing direct access to SC and the CCE. TM motion provides a means of identifying functional regions of the outflow system that are of particular interest because, to function, such regions must have participation of the adjacent more distal outflow pathways.[35,36] Because there is little circumferential flow in SC, accurate placement of MIGS adjacent to CCE within SC is likely to be highly important to the success of such procedures.

In summary, PhS-OCT, a phase-based OCT approach, is feasible to quantify pulse-induced TM motion in humans in vivo. The approach demonstrates high repeatability and reliability. The ability to quantitate TM motion may prove to be a promising tool to help identify, monitor, and potentially guide treatment for glaucoma patients.

Acknowledgments

Supported in part by grants from Washington Research Foundation, the National Eye Institute (Grant R01EY024158), Carl Zeiss Meditec, Inc., and an unrestricted grant from the Research to Prevent Blindness, Inc., (New York, NY, USA). The funding organization had no role in the design or conduct of this research.

Disclosure: **C. Xin**, None; **S. Song**, None; **M. Johnstone**, None; **N. Wang**, None; **R.K. Wang**, None

References

1. Johnstone MA. The aqueous outflow system as a mechanical pump: evidence from examination of tissue and aqueous movement in human and non-human primates. *J Glaucoma*. 2004;13:421–438.
2. Xin C, Wang RK, Song S, et al. Aqueous outflow regulation: optical coherence tomography implicates pressure-dependent tissue motion. *Exp Eye Res*. 2017;158:171–186.

3. Carreon T, van der Merwe E, Fellman RL, Johnstone M, Bhattacharya SK. Aqueous outflow: a continuum from trabecular meshwork to episcleral veins. *Prog Retin Eye Res*. 2017;57:108–133.
4. Ascher KW. The search for aqueous veins. *Am J Ophthalmol*. 1948;31:105.
5. Ascher KW. When were the aqueous veins detected? *Am J Ophthalmol*. 1952;35:1512–1514.
6. Johnstone M, Martin E, Jamil A. Pulsatile flow into the aqueous veins: manifestations in normal and glaucomatous eyes. *Exp Eye Res*. 2011;92:318–327.
7. Huang AS, Li M, Yang D, Wang H, Wang N, Weinreb RN. Aqueous angiography in living nonhuman primates shows segmental, pulsatile, and dynamic angiographic aqueous humor outflow. *Ophthalmology*. 2017;124:793–803.
8. Ye W, Gong H, Sit A, Johnson M, Freddo TF. Interendothelial junctions in normal human Schlemm's canal respond to changes in pressure. *Invest Ophthalmol Vis Sci*. 1997;38: 2460–2468.
9. Stamer WD, Braakman ST, Zhou EH, et al. Biomechanics of Schlemm's canal endothelium and intraocular pressure reduction. *Prog Retin Eye Res*. 2015;44:86–98.
10. Vranka JA, Kelley MJ, Acott TS, Keller KE. Extracellular matrix in the trabecular meshwork: intraocular pressure regulation and dysregulation in glaucoma. *Exp Eye Res*. 2015;133:112–125.
11. Raghunathan VK, Morgan JT, Park SA, et al. Dexamethasone stiffens trabecular meshwork, trabecular meshwork cells, and matrix. *Invest Ophthalmol Vis Sci*. 2015;56:4447–4459.
12. Raghunathan VK, Morgan JT, Dreier B, et al. Role of substratum stiffness in modulating genes associated with extracellular matrix and mechanotransducers YAP and TAZ. *Invest Ophthalmol Vis Sci*. 2013;54:378–386.
13. Wang K, Johnstone MA, Xin C, et al. Estimating human trabecular meshwork stiffness by numerical modeling and advanced OCT imaging. *Invest Ophthalmol Vis Sci*. 2017;58: 4809–4817.
14. Liu B, McNally S, Kilpatrick JI, Jarvis SP, O'Brien CJ. Aging and ocular tissue stiffness in glaucoma. *Surv Ophthalmol*. 2018; 63:56–74.
15. Wang RK, Ma Z, Kirkpatrick SJ. Tissue Doppler optical coherence elastography for real time strain rate and strain mapping of soft tissue. *Appl Phys Lett*. 2006;89:144103.
16. Wang RK, Nuttall AL. Phase-sensitive optical coherence tomography imaging of the tissue motion within the organ of Corti at a subnanometer scale: a preliminary study. *J Biomed Optics*. 2010;15:056005.
17. Li P, Reif R, Zhi Z, Martin E, Shen TT, Johnstone M, Wang RK. Phase sensitive optical coherence tomography characterization of pulse-induced trabecular meshwork displacement in ex vivo nonhuman primate eyes. *J Biomed Opt*. 2012;17: 076026.
18. Li P, Shen TT, Johnstone M, Wang RK. Pulsatile motion of the trabecular meshwork in healthy human subjects quantified by phase-sensitive optical coherence tomography. *Biomed Opt Express*. 2013;4:2015–2065.
19. Clark AF, Wilson K, McCartney MD, Miggans ST, Kunkle M, Howe W. Glucocorticoid-induced formation of cross-linked actin networks in cultured human trabecular meshwork cells. *Invest Ophthalmol Vis Sci*. 1994;35:281–294.
20. Filla MS, Schwinn MK, Nosie AK, Clark RW, Peters DML. Dexamethasone-associated cross-linked actin network formation in humantrabecular meshwork cells involves β3 integrin signaling. *Invest Ophthalmol Vis Sci*. 2011;52:2952–2959.
21. Yuan Y, Call MK, Yuan Y, Fischesser K, Liu CY, Kao WW. Dexamethasone induces crosslinked actin networks in trabecular meshwork cells through noncanonical wnt signaling. *Invest Ophthalmol Vis Sci*. 2013;54:6502–6509.
22. Johnstone MA. The aqueous outflow system as a mechanical pump: evidence from examination of tissue and aqueous movement in human and non-human primates. *J Glaucoma*. 2004;13:421–438.
23. Johnstone MA. A new model describes an aqueous outflow pump and explores causes of pump failure in glaucoma. In: Grehn F, Stamper R, eds. *Glaucoma. Essentials in Ophthalmology*. Berlin: Springer; 2006:3–34.
24. Johnstone MA. Aqueous humor outflow system overview. In: Krieglstein GK, Weinreb RN, eds. *Becker-Shaffer's Diagnosis and Therapy of the Glaucomas*. Berlin: Springer; 2009:25–46.
25. Johnstone M, Martin E, Jamil A. Pulsatile flow into the aqueous veins: manifestations in normal and glaucomatous eyes. *Exp Eye Res*. 2011;92:318–327.
26. Uchida T, Honjo M, Yamagishi R, Aihara M. The anti-inflammatory effect of ripasudil (K-115), a rho kinase (ROCK) inhibitor, on endotoxin-induced uveitis in rats. *Invest Ophthalmol Vis Sci*. 2017;58:5584–5593.
27. Pillunat LE, Erb C, Jünemann AG, Kimmich F. Micro-invasive glaucoma surgery (MIGS): a review of surgical procedures using stents. *Clin Ophthalmol*. 2017;11:1583–1600.
28. Ueda J, Yue BY. Distribution of myocilin and extracellular matrix components in the corneoscleral meshwork of human eyes. *Invest Ophthalmol Vis Sci*. 2003;44:4772–4779.
29. Huang AS, Gonzalez JM Jr, Le PV, Heur M, Tan JC. Sources of structural autofluorescence in the human trabecular meshwork. *Invest Ophthalmol Vis Sci*. 2013;54:4813–4820.
30. Park CY, Lee JK, Kahook MY, Schultz JS, Zhang C, Chuck RS. Revisiting ciliary muscle tendons and their connections with the trabecular meshwork by two photon excitation microscopic imaging. *Invest Ophthalmol Vis Sci*. 2016;57:1096–1105.
31. Hann CR, Springett MJ, Wang X, Johnson DH. Ultrastructural localization of collagen IV, fibronectin, and laminin in the trabecular meshwork of normal and 353 glaucomatous eyes. *Ophthalmic Res*. 2001;33:314–324.
32. Pattabiraman PP, Rao PV. Hic-5 regulates actin cytoskeletal reorganization and expression of fibrogenic markers and myocilin in trabecular meshwork cells. *Invest Ophthalmol Vis Sci*. 2015;56:5656–5669.
33. Saccà SC, Gandolfi S, Bagnis A, et al. The outflow pathway: a tissue with morphological and functional unity. *J Cell Physiol*. 2016;231:1876–1893.
34. Osmond M, Bernier SM, Pantcheva MB, Krebs MD. Collagen and collagen chondroitin sulfate scaffolds with uniaxially aligned pores for the biomimetic, three dimensional culture of trabecular meshwork cells. *Biotechnol Bioeng*. 2017;114: 915–923.
35. Tellios N, Belrose JC, Tokarewicz AC, et al. TGF-β induces phosphorylation of phosphatase and tensin homolog: implications for fibrosis of the trabecular meshwork tissue in glaucoma. *Sci Rep*. 2017;7:812.
36. Battista SA1, Lu Z, Hofmann S, Freddo T, Overby DR, Gong H. Reduction of the available area for aqueous humor outflow and increase in meshwork herniations into collector channels following acute IOP elevation in bovine eyes. *Invest Ophthalmol Vis Sci*. 2008;49:5346–5352.
37. Zhang Y, Toris CB, Liu Y, Ye W, Gong H. Morphological and hydrodynamic correlates in monkey eyes with laser induced glaucoma. *Exp Eye Res*. 2009;89:748–756.
38. Hamanaka T. Scleral spur and ciliary muscle in man and monkey. *Jpn J Ophthalmol*. 1989;33:221–236.
39. Lütjen-Drecoll E, Kaufman PL, Bárány EH. Light and electron microscopy of the anterior chamber angle structures following surgical disinsertion of the ciliary muscle in the cynomolgus monkey. *Invest Ophthalmol Vis Sci*. 1977;16: 218–225.

Investigative Ophthalmology & Visual Science

40. Kaufman PL, Bárány EH. Loss of acute pilocarpine effect on outflow facility following surgical disinsertion and retrodisplacement of the ciliary muscle from the scleral spur in the cynomolgus monkey. *Invest Ophthalmol Vis Sci*. 1976;15:793–807.
41. Thieme H, Nass JU, Nuskovski M, Wiederholt M. The effects of the carbonic anhydrase inhibitors methazolamide, diclofenamide and dorzolamide on trabecular meshwork and ciliary muscle contractility. *Exp Eye Res*. 1999;69:455–458.
42. Wiederholt M, Thieme H, Stumpff F. The regulation of trabecular meshwork and ciliary muscle contractility. *Prog Retin Eye Res*. 2000;19:271–295.
43. Overby DR, Bertrand J, Schicht M, Paulsen F, Stamer WD, Lutjen-Drecoll E. The structure of the trabecular meshwork, its connections to the ciliary muscle, and the effect of pilocarpine on outflow facility in mice. *Invest Ophthalmol Vis Sci*. 2014;55:3727–3736.
44. Kronfeld PC. Further gonioscopic studies on the canal of Schlemm. *Arch Ophthalmol*. 1949;41:393–405.
45. Suson EB, Schultz RO. Blood in schlemm's canal in glaucoma suspects. A study of the relationship between blood-filling pattern and outflow facility in ocular hypertension. *Arch Ophthalmol*. 1969;81:808–812.
46. Phelps CD, Asseff CF, Weisman RL, Podos SM, Becker B. Blood reflux into Schlemm's canal. *Arch Ophthalmol*. 1972;88:625–631.
47. Ascher KW. Aqueous veins: II. Local pharmacologic effects on aqueous veins III. Glaucoma and the aqueous veins. *Am J Ophthamol*. 1949;25:1301–1315.
48. De Vries S. *De Zichtbare Afvoer Van Het Kamerwater*. Amsterdam: Drukkerij Kinsbergen; 1947.
49. Thomassen TL. The venous tension of eyes suffering from simple glaucoma. *Acta Ophthamol*. 1947;25:221–241.
50. Cambiaggi A. Effeto della jaluronidasi sulla pressone intraoculare e sull'asetto della vene dell'accqueo. *Boll Soc Biol Sper*. 1958;34:1–7.

Investigative Ophthalmology & Visual Science